

RESEARCH ARTICLE

10.1002/2017JD026510

Highly variable aerodynamic roughness length (z_0) for a hummocky debris-covered glacierEvan S. Miles^{1,2} , Jakob F. Steiner³ , and Fanny Brun⁴ 

Key Points:

- Aerodynamic roughness length (z_0) is highly variable for hummocky debris-covered glaciers, ranging from 0.005 m to 0.5 m
- Theoretical and empirical microtopographic methods correlate but differ in magnitude (4X) and are sensitive to scale of analysis
- Aerodynamically derived values of z_0 (0.03–0.05 m) represent smoother surface character for this complex terrain

Correspondence to:

E. S. Miles,
evan.s.miles@cantab.net

Citation:

Miles, E. S., J. F. Steiner, and F. Brun (2017), Highly variable aerodynamic roughness length (z_0) for a hummocky debris-covered glacier, *J. Geophys. Res. Atmos.*, 122, 8447–8466, doi:10.1002/2017JD026510.

Received 16 JAN 2017

Accepted 29 JUN 2017

Accepted article online 23 JUL 2017

Published online 23 AUG 2017

¹Scott Polar Research Institute, University of Cambridge, Cambridge, UK, ²School of Geography, University of Leeds, Leeds, UK, ³Department of Physical Geography, Universiteit Utrecht, Utrecht, Netherlands, ⁴University Grenoble Alpes, CNRS, IRD, LTHE, Grenoble, France

Abstract The aerodynamic roughness length (z_0) is an essential parameter in surface energy balance studies, but few literature values exist for debris-covered glaciers. We use microtopographic and aerodynamic methods to assess the spatial variability of z_0 for Lirung Glacier, Nepal. We apply structure from motion to produce digital elevation models for three nested domains: five 1 m² plots, a 21,300 m² surface depression, and the lower 550,000 m² of the debris-mantled tongue. Wind and temperature sensor towers were installed in the vicinity of the plots within the surface depression in October 2014. We calculate z_0 according to a variety of transect-based microtopographic parameterizations for each plot, then develop a grid version of the algorithms by aggregating data from all transects. This grid approach is applied to the surface depression digital elevation model to characterize z_0 spatial variability. The algorithms reproduce the same variability among transects and plots, but z_0 estimates vary by an order of magnitude between algorithms. Across the study depression, results from different algorithms are strongly correlated. Using Monin-Obukov similarity theory, we derive z_0 values from the meteorological data. Using different stability criteria, we derive median values of z_0 between 0.03 m and 0.05 m, but with considerable uncertainty due to the glacier's complex topography. Considering estimates from these algorithms, results suggest that z_0 varies across Lirung Glacier between ~0.005 m (gravels) to ~0.5 m (boulders). Future efforts should assess the importance of such variable z_0 values in a distributed energy balance model.

1. Introduction

Debris-covered glaciers are distributed globally, representing a distinctive minority of total glacier area. Although debris-covered glaciers have received focused study in recent years, the interactions of a debris-covered glacier with the atmosphere are complex and some physical processes remain poorly understood [Brock *et al.*, 2010; Collier *et al.*, 2014, 2015; Rounce *et al.*, 2015; Evatt *et al.*, 2015]. Debris cover heavily modifies the primary processes of energy exchange between the atmosphere and the glacier surface. Early studies identified the thickness-dependent trade-off between albedo and conductive heat transfer [Østrem, 1959], but the debris surface also has direct effects on the longwave radiation budget and turbulent energy exchange [Collier *et al.*, 2014; Evatt *et al.*, 2015; Steiner *et al.*, 2015], while the presence of supraglacial debris has been noted to heighten temperature lapse rates at the glacier scale [Steiner and Pellicciotti, 2016; Shaw *et al.*, 2015].

Studies have increasingly incorporated these processes into point scale models of subdebris melt [e.g., Nicholson and Benn, 2006; Brock *et al.*, 2010; Fyffe *et al.*, 2014; Evatt *et al.*, 2015]. In addition to meteorological forcing, energy balance models require knowledge of the debris layer's properties, including debris thickness, effective thermal conductivity, albedo, and aerodynamic roughness length. It is possible to constrain these parameters at a point through extensive field observations [Ragetti *et al.*, 2015] or to estimate them through model optimization [Rounce *et al.*, 2015]. However, each of these parameters is spatially variable and largely unconstrained for a debris-covered glacier surface, so distributed applications of a debris-covered glacier energy balance model are rare [Reid *et al.*, 2012; Fyffe *et al.*, 2014; Collier *et al.*, 2015].

This paper explores one important parameter, the aerodynamic roughness length, to understand its spatial variability. We first examine existing literature on the topic to structure our aims for the study.

1.1. Background

The term “surface roughness” has many technical meanings and applications in the earth sciences, but here we consider specifically the aerodynamic roughness length ($z_{0,M}$, hereafter z_0), defined as the height above

the ground at which a vertical wind profile drops to zero [Smith, 2014]. Analytically, the term is a constant of integration from the log profile of turbulent flow velocity over a surface, and this characterizes the loss of wind momentum due to the surface's fine topographic variability [Chappel and Heritage, 2007]. Thus, z_0 by definition directly influences the turbulent exchanges of sensible and latent energy at a surface and is a crucial parameter in energy balance models [e.g., Reid and Brock, 2010; Fyffe et al., 2014].

Applying Monin-Obukhov similarity theory, z_0 can be determined at a point by fitting a logarithmic curve to an observed wind profile [e.g., Brock et al., 2006; Smeets and van den Broeke, 2008a]. Alternatively, wind tunnel measurements provide robust estimates of z_0 by repeatedly perturbing a steady flow with regular roughness elements [Counihan, 1971; Petersen, 1997]. However, both of these methods are difficult to apply to complex terrain exhibiting irregular roughness elements, such as a debris-covered glacier: as these values of z_0 integrate terrain and flow interactions over an unknown distance, they are intended to be collected with a long fetch of relatively homogeneous terrain. Nonetheless, similarity theory has been found valid for some examples of complex terrain [Smeets et al., 1999], but the need for near-surface stability [Martins et al., 2009] and often moderate wind speeds [Liang et al., 2014], can greatly limit the number of observations of this kind.

Research has also attempted to construct physically plausible parameterizations of z_0 based on the geometry of roughness elements and their effective drag for a turbulent flow, using both mechanistic models based on the drag of elements [e.g., Lettau, 1969; Counihan, 1971; Munro, 1989; Rounce et al., 2015; Smith et al., 2015b] and empirical relationships developed from wind tower measurements [Nield et al., 2013a]. These microtopographic methods have proven effective for capturing the variability of roughness between sites and transect directions [Rees and Arnold, 2006; Nield et al., 2013a; Irvine-Fynn et al., 2014]. Traditional microphotographic methods rely on measurements of elevation along a transect, then estimation of an effective roughness element and the corresponding z_0 value [e.g., Lettau, 1969; Munro, 1989].

More recently, the ability to collect very high resolution and accurate terrain data through Light Detection And Ranging (LiDAR) [e.g., Nield et al., 2013b] and structure from motion (SfM) (see Smith et al. [2015a] for a review of the technology and a comprehensive overview of recent literature) has inspired application of microtopographic methods to gridded data sets or point clouds. However, microtopographic methods are difficult to apply uniformly between studies: transect approaches [e.g., Rees and Arnold, 2006] and grid or point cloud-based efforts [Nield et al., 2013b; Irvine-Fynn et al., 2014; Rounce et al., 2015; Smith et al., 2015b] differ in scale of analysis and resolution. Further, the sensitivity of microtopographic algorithms to numerous parameters remains unclear, including the following: transect length, resolution, size of a detectable obstacle, and detrending method. Perhaps most importantly, many of the recent methods have been developed without in situ wind observation to validate the microtopographic estimates of z_0 [Irvine-Fynn et al., 2014; Rounce et al., 2015; Smith et al., 2015b]. Consequently, empirical relationships probably best represent actual values of z_0 as they are developed from paired wind and topographic measurements spanning several orders of magnitude of roughness [Nield et al., 2013b].

Reported values of z_0 for glacier surfaces span several orders of magnitude, with reported values ranging from 4×10^{-4} m for dry snow on an ice sheet to 8×10^{-2} m for very rough glacier surfaces [Brock et al., 2006; Smeets and van den Broeke, 2008b; Guo et al., 2011]. Microtopographic observations have been able to reproduce much of this variability (Table 1). For snow and ice surfaces, studies have noted a strong difference in microtopographic estimates for cross-glacier and down-glacier survey directions partly due to feedback between wind in the dominant flow direction and surface change [Brock et al., 2006; Rees and Arnold, 2006; Irvine-Fynn et al., 2014].

For surfaces similar to a debris-covered glacier in composition, z_0 estimates range between 5×10^{-4} m and 9.8×10^{-2} m, increasing strongly with the portion of a surface covered by debris and with the size of typical debris grains (Table 1). Relatively few studies have estimated z_0 for a debris-covered glacier surface, so here we also include measurements for other rocky surfaces. Values actually used in energy balance models for debris-covered glaciers comprise a much smaller window of the measured range (Table 2). A theoretical minimum value of z_0 can be established by the surface variations of a boulder Dabski [2012], while most estimates fall in the range 5×10^{-3} m to 2×10^{-2} m. For modeling applications, the values are generally applied as a uniform fixed value, although roughness is known to vary in space [Rippin et al., 2015] and time [Nield et al., 2013a].

Table 1. Values of z_0 Reported by Previous Studies, Distinguishing Between Aerodynamic and Microtopographic Approaches as Applied to Clean Ice and Heterogeneous Rocky Surfaces

Study	Approach	Method	Surface	z_0 (m)	Site
Brock et al. [2006]	Aerodynamic	Literature review	Fresh snow	0.0002	Various
			Snow	0.0009–0.0016	
			Penitentes	0.003	
			Glacier ice	0.0001–0.0027	
			Very rough glacier ice	0.0058–0.08	
			Ice sheet, dry snow	0.00004–0.001	
Brock et al. [2006]	Aerodynamic	Wind profile	Melting snow/sastrugi	0.001–0.0135	
			Ice sheet, bare ice	0.00007–0.0067	
			Snow	0.00356	
			Slush	0.00088	
Brock et al. [2006]	Microtopography	String profiles [Lettau, 1969]	Bare ice	0.00689	
			Snow (down-glacier)	0.00162	
Rees and Arnold [2006]	Microtopography	Photogrammetry [Munro, 1989]	Snow (cross-glacier)	0.00231	
			Slush	0.00065	
			Clean ice (down-glacier)	0.00088	
Rees and Arnold [2006]	Microtopography	String profile [Munro, 1989]	Clean ice (cross-glacier)	0.00696	
			Clean ice (down-glacier)	0.00033	
Irvine-Fynn et al. [2014]	Microtopography	Photogrammetry 1 m ² [Lettau, 1969]	Clean ice (cross-glacier)	0.00056	
			Clean ice (down-glacier)	0.00212	
Irvine-Fynn et al. [2014]	Microtopography	Photogrammetry 4 m ² [Lettau, 1969]	Clean ice (cross-glacier)	0.00216	
			Clean ice (down-glacier)	0.0001–0.001	
Inoue and Yoshida [1980]	Aerodynamic	Wind profile	Clean ice (cross-glacier)	0.0005–0.0031	
			Clean ice (down-glacier)	0.0004–0.0008	
Takeuchi et al. [2000]	Aerodynamic	Wind profile	Clean ice (cross-glacier)	0.0007–0.0021	
			Clean ice (down-glacier)	0.06	
Dong et al. [2002]	Aerodynamic	Wind tunnel	Large debris	0.0035	
			Small debris with bare ice	0.0063	
Brock et al. [2007]	Aerodynamic	Sensitivity testing	Debris-covered glacier	0.00214–0.0106	
			Gravels of varying size	0.0005–0.005	
Nield et al. [2013a]	Aerodynamic	Wind profile	Volcanic tephra	0.016	
			Debris-covered glacier	0.0008–0.003	
Wang et al. [2014]	Aerodynamic	Eddy covariance and wind profile	Volcanic tephra	0.00075	
			Moraine, with snow	0.093–0.098	
Rounce et al. [2015]	Microtopography	Photogrammetry 4 m ² [Munro, 1989]	Moraine	0.0022–0.0091	
			Debris-covered glacier	0.007–0.03	
Dabski [2012]	Microtopography	Electronic profilometer	Debris-covered glacier	4.03–8.54 × 10 ^{−6}	
			Surface of a boulder	Icelandic and Swiss glacier forefields	

Table 2. Values of z_0 Used in Modeling the Energy Balance of the Debris-Covered Glacier Surface

Study	z_0 (m)	Source
<i>Nicholson and Benn</i> [2006]	0.01	<i>Takeuchi et al.</i> [2000]
<i>Reid and Brock</i> [2010]	0.016	<i>Brock et al.</i> [2010]
<i>Reid et al.</i> [2012]	0.016	<i>Brock et al.</i> [2010]
<i>Lejeune et al.</i> [2013]	0.012	assumed
<i>Collier et al.</i> [2014]	0.016	<i>Brock et al.</i> [2010]
<i>Fyffe et al.</i> [2014]	0.016	<i>Brock et al.</i> [2010]
<i>Fujita and Sakai</i> [2014]	0.005	calibration parameter
<i>Ragettli et al.</i> [2015]	0.016	<i>Brock et al.</i> [2010]
<i>Evatt et al.</i> [2015]	0.01	<i>Nicholson and Benn</i> [2006]
<i>Rounce et al.</i> [2015]	0.007–0.03	optimized

Relatively few studies have assessed the aerodynamic roughness length on the Tibetan Plateau or the Himalaya, and even fewer have done so for glaciers. In the Tibetan Plateau, *Guo et al.* [2011] measured z_0 varying between 10^{-4} and 10^{-2} m over a changing glacier surface during the ablation season. In the Himalaya, *Azam et al.* [2014] calculated z_0 over a changing glacier surface based on wind measurements at two heights, resulting in $z_0 = 0.016$ for ice and 0.001 for snow surfaces. *Inoue and Yoshida* [1980] and *Wang et al.* [2014] have provided the only measurements of z_0 on a debris-covered glacier in the region to date (Table 1). Other data frequently used in energy balance studies in the region stem from experiments carried out on multiple off-glacier sites [*Yang et al.*, 2002].

It is conclusively important to note that although aerodynamic and microtopographic estimates of z_0 can be compared, they are actually measuring different things: a property of a flow and of a surface, respectively [*Smith*, 2014].

1.2. Aim of This Study

This study aspires to advance understanding of the variability of aerodynamic roughness lengths for a debris-covered glacier by pursuing several lines of inquiry. In this analysis, we

1. Estimate z_0 with transect-based microtopographic methods for five plots on a hummocky debris-covered glacier to determine sensitivity of algorithms to input data and to determine isotropy of the debris surface.
2. Estimate z_0 using empirical and mechanistic microtopographic methods for larger domains (within a typical surface depression and across the whole debris-covered glacier tongue), to determine a range of values for use in optimization and modeling.
3. Calculate z_0 within the study area based on aerodynamic inversion of wind observations and compare this to the estimates at plot, basin, and glacier scales.
4. Compare the aerodynamic estimate of z_0 to microtopographic estimates based on varying DEM sizes to consider the utility of the microtopographic methods.

2. Field Observations

In October 2014 a field campaign collected data to estimate z_0 for the debris-covered Lirung Glacier in Nepal.

2.1. Study Site

Lirung Glacier (28° 13' 57" N, 85° 33' 43" E) is located in the upper Langtang River catchment of Nepal (Figure 1a), and is one of several debris-covered glaciers in the valley. Lirung Glacier has a very large elevation range (~4000–7132 m above sea level, asl), beginning near the summit of Langtang Lirung and flowing south and has a total area of about 6 km² [*Ragettli et al.*, 2015].

The glaciers in the Langtang Valley are rapidly thinning in response to climate change [*Pellicciotti et al.*, 2015], and Lirung Glacier specifically is in an advanced state of decay. In recent decades the glacier's low-gradient tongue detached from the headwall accumulation area and a proglacial lake formed at the glacier's terminus. The glacier has retreated 1.4 km from this position [*Immerzeel et al.*, 2014] and has thinned dramatically from its Little Ice Age moraines [*Miles et al.*, 2017b].

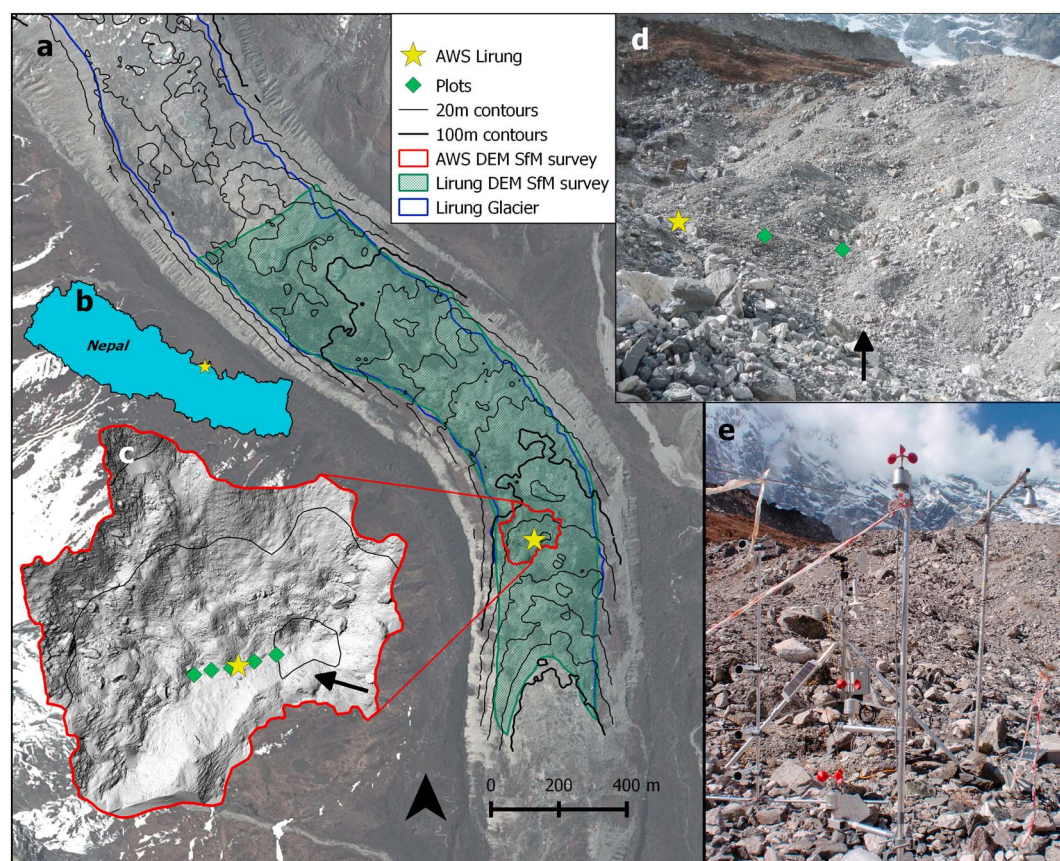


Figure 1. (a) Location of the AWS and survey areas on Lirung Glacier. (b) Location within Nepal. (c) Hillshade of the 5 cm resolution DEM derived for the study depression, also showing locations of the 1 m² plots and meteorological equipment. (d) Ground view of the study depression, study plots, and meteorological stations, highlighting the range of grain sizes and local topographic variability of the debris surface. (e) Configuration of wind and temperature sensor tower and automated weather station on Lirung Glacier.

Currently, more than 20% of the Lirung Glacier's surface is mantled with rocky debris, which extends to 5200 m asl. The debris-covered glacier tongue has a length of 3.5 km and averages 500 m in width, although the transition between debris-covered glacier and ice-cored lateral moraine is difficult to demarcate (Figure 1a). The debris layer exceeds 50 cm in thickness for most of this area [Ragetti *et al.*, 2015], and the debris is very heterogeneous in composition, ranging from boulders with several meters in height to fine silts (Figure 1c). The surface topography of the debris-covered tongue exhibits extremely variable relief characterized by ablation-induced debris cones and depressions and is punctuated by occasional cliffs of bare ice [Steiner *et al.*, 2015; Brun *et al.*, 2016] and surface ponds [Miles *et al.*, 2017b].

2.2. Plot Surveys

Five 1 m² plots were surveyed to represent the variety of surface conditions on the debris-covered tongue. Plots were located within 20 m of an automated weather station (AWS) and wind tower (Figure 1). For scale, a right angle meterstick was placed at the plot, then five photographs were taken to observe the plot from each cardinal direction and overhead.

Agisoft Photoscan software was then used to process the photographs into a digital elevation model (DEM) and synthetic orthophoto for each plot. Photoscan uses structure from motion (SfM) to solve for a surface point cloud from disperse photographs. SfM is increasingly used in cryospheric studies [Irvine-Fynn *et al.*, 2014; Rounce *et al.*, 2015; Brun *et al.*, 2016], and the reader is directed to Westoby *et al.* [2012] for a description of the SfM workflow and Immerzeel *et al.* [2014] for Agisoft specifically. The meterstick ends and corners were used to locally georeference the plot, then the meterstick was measured in Agisoft at 10 cm increments to evaluate the inherent errors in the terrain model. The mean absolute error for these positions was 1 mm horizontally and 1.5 mm vertically. Each plot's point cloud was gridded to a DEM of 1 mm horizontal resolution for analysis.

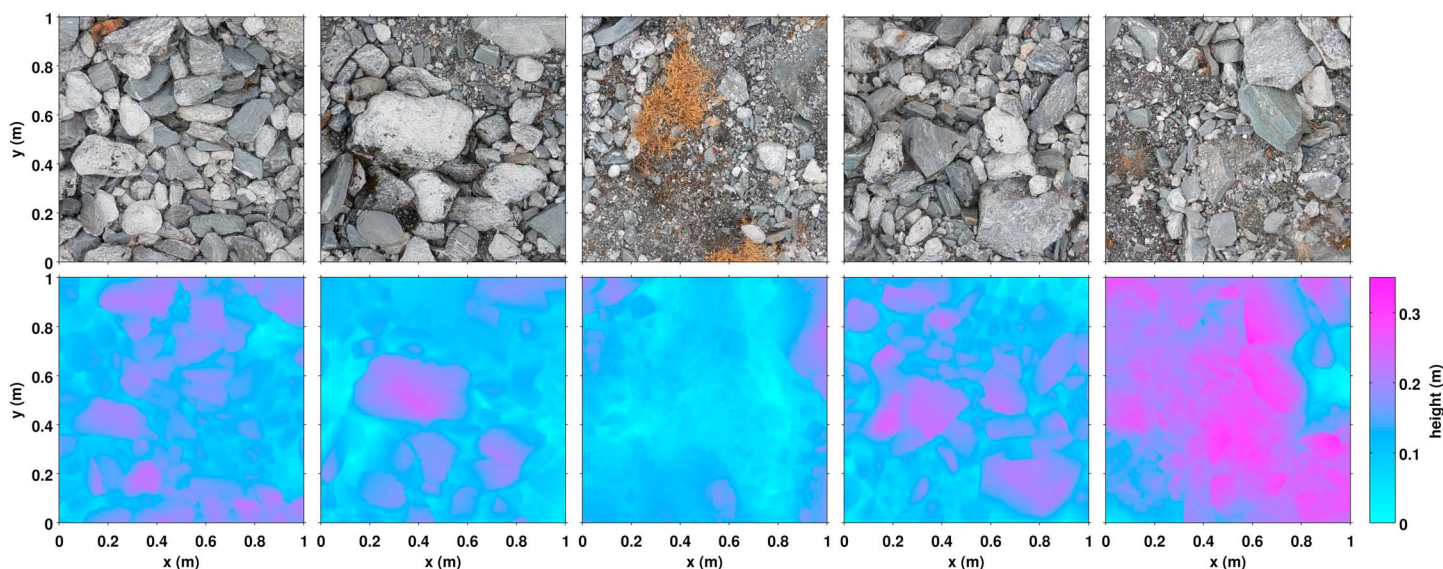


Figure 2. (top) SfM-generated orthophotos and (bottom) detrended DEMs for the five study plots highlight the variable composition of the debris surface. Up-glacier is oriented upward for each plot.

The resulting DEMs and synthetic orthophotos are displayed in Figure 2, showing surface conditions typical of Lirung Glacier, including sporadic vegetation.

2.3. SfM Surveys of the Glacier Tongue

At the opposite extreme of scales, a terrestrial SfM survey was completed to develop a DEM covering the majority of the debris-mantled tongue (550,000 m²), using 737 photographs taken from the glacier's lateral moraines and from prominent positions on the glacier surface. The point cloud generated from these data was gridded to 25 cm resolution. These data (hereafter, Lirung DEM) were evaluated with 682 differential global positioning system (dGPS) points taken on the glacier surface and had a mean absolute error of 0.5 m [Brun, 2015]. Comparable SfM-generated DEMs have previously been derived for this area from airborne surveys [Immerzeel *et al.*, 2014; Kraaijenbrink *et al.*, 2016].

Finally, a similar survey was completed for a local surface depression, consisting of 173 terrestrial photographs taken in the proximity of the AWS. These photographs were processed using Agisoft to produce a DEM for the surveyed area (approximately 41,000 m²) at 5 cm horizontal resolution based on the geometric agreement of the point cloud (18 million points). Hereafter, this is referred to as the AWS DEM. To assess the accuracy of this 5 cm DEM (hereafter, AWS DEM), it was compared to the Lirung DEM. After georeferencing and trimming to the area with a consistent high density of points with few interpolation zones, the AWS DEM covered 21,300 m² (Figure 1b). For this area, the standard deviation of elevation differences between the AWS DEM and Lirung DEM is 1.2 m, which is largely due to the representation of large boulders (>4 m tall) at the site, which were not delineated as clearly at the coarser resolution.

Individual boulders in the depression extend up to 10 m in height and length, while a few patches that could not be adequately resolved with our photos appear as smooth areas due to interpolation. Most of the depression's debris surface is composed of cobbles similar in size to the study plots (Figure 1c).

2.4. Wind and Temperature Towers

An AWS was located on the debris-covered tongue from 2012 until it was destroyed by the Gorkha earthquake in April 2015 (4076 m asl, see Figure 1 for locations and Steiner *et al.* [2015] for details). For a period of 11 days in October 2014, towers were erected adjacent to the AWS and equipped with sensors to measure air temperature and wind speed. Air temperature was measured at the surface, 20 cm, 50 cm, 1 m, and 2 m above the ground using Onset TidBits (UTBI-001, accuracy: $\pm 0.2^\circ\text{C}$) shielded from direct radiation with PVC pipes coated in aluminum foil. Anemometers (Anderaa Wind Speed Sensor 2740, accuracy: $\pm 2\%$) were used to measure wind speed at 50 cm, 1 m, and 2 m heights, while wind direction was recorded by the AWS. Reported heights are measured from the base of the towers, which is a flat plate that rests atop the surface. Temperature and wind speed were recorded at 5 min intervals and averaged to 30 min values for analysis.

3. Analysis

To capture the variability of z_0 across our study site, and in an effort to constrain its magnitude, we use a combination of mechanistic and empirical microtopographic models. These methods are first applied in the traditional transect approach, then applied in an approach suitable for gridded data. We then compare these values to z_0 calculated from aerodynamic inversion at the AWS location.

3.1. Microtopographic Transect Approach

First, we analyze the microtopography of the study plots using profiles of elevation data. Several mechanistic methods to estimate z_0 have been developed based on the zero-up-crossing approach of *Lettau* [1969]. A linear set of height measurements is detrended and broken into sections crossing the mean value in an upward direction. Each of these sections is considered an obstacle to wind, and its length and height are measured, forming a population of obstacles. The method of *Lettau* [1969] then estimates the resistance to flow based on the average obstacle size, h^* , with equation (1), where s is the silhouette area of the average obstacle or vertical crosswind-lateral plane (cm^2) and S the specific area measured in the horizontal plane (cm^2). Employing *Lettau's* nomenclature, s and S are defined by equations (2) and (3), where X is the length of the transect and f is the number of continuous groups of positive height deviations above the mean elevation.

$$z_0 = 0.5h^* \frac{S}{s} \quad (1)$$

$$s = \frac{h^*X}{2f} \quad (2)$$

$$S = \left(\frac{X}{f}\right)^2 \quad (3)$$

$$z_0 = \frac{\sigma_z^2 f}{X} \quad (4)$$

Numerous alternative microtopographic methods are available from the literature, but we use algorithms from two sources. The method of *Munro* [1989] has been used extensively in glaciology and is an approximation to the method of *Lettau* [1969] using twice the standard deviation of elevation for the detrended profile rather than the mean obstacle height ($h^* = 2\sigma_z$), which reduces equations (1)–(3) to equation (4). Meanwhile, *Nield et al.* [2013b] combined wind tower measurements with terrestrial laser scanning of small plots to develop empirical relationships between z_0 and diverse surface characteristics.

To calculate z_0 , we use the *Lettau* [1969] (hereafter, *Lettau*) and *Munro* [1989] (*Munro*) profile methods, as well as select best fit empirical parameterizations from *Nield et al.* [2013a], based on the following: the standard deviation of bilinearly detrended surface elevations (*NieldEstd*, equation (5)), the standard deviation of obstacle heights (*NieldHstd*, equation (6)), the mean obstacle height (*NieldHmean*, equation (7)), the maximum obstacle height (*NieldHmax*, equation (8)) encountered for the profile, and the sill of a fitted semivariogram for a profile of elevations (*NieldSill*, equation (9)). Many other empirical parameterizations are developed in *Nield et al.* [2013b], but we chose to evaluate single-parameter models with $R^2 > 0.7$.

$$\ln(z_0) = 0.65 + 1.37 \times \ln(\sigma_z); \quad (5)$$

$$\ln(z_0) = 0.28 + 1.33 \times \ln(h_\sigma); \quad (6)$$

$$\ln(z_0) = -0.29 + 1.33 \times \ln(h_{\text{mean}}); \quad (7)$$

$$\ln(z_0) = -2.02 + 1.5 \times \ln(h_{\text{max}}); \quad (8)$$

$$\ln(z_0) = 0.6 + 0.67 \times \ln(s); \quad (9)$$

For equations (5) to (9), σ_z is the standard deviation of bilinearly detrended surface elevations (m), h_σ is the standard deviation of obstacle heights (m), h_{mean} is the mean obstacle height (m), h_{max} is the maximum

obstacle height (m) for the profile and s is the sill (m^2) of a fitted semivariogram for a profile of elevations [Nield *et al.*, 2013b].

With a spatial resolution of 1 mm and extent of 1 m, each plot DEM produces 1001 profiles of 1001 elevations for down-glacier and cross-glacier directions (i.e., each row and column). To estimate z_0 by these profile methods, we evaluate the algorithms for each plot's profiles in down-glacier and cross-glacier directions. We then evaluate the anisotropic ratio of z_0 values for each algorithm and plot.

3.2. Microtopographic Grid Approach

Second, to calculate z_0 from the AWS DEM, we developed a gridded implementation of the profile methods. For a detrended DEM of equal height and width, we determined the standard deviation of elevations, from which the NieldEstd method was used to directly estimate z_0 . We then aggregated obstacles from all detrended profiles in the down-glacier and cross-glacier directions, both forward and backward, to characterize the full distribution of potential obstacles with which the boundary layer interacts. We then applied each of the profile methods (NieldHstd, NieldHmean, NieldHmax, and Lettau, Munro) to the combined obstacle population.

Thus, to estimate z_0 across the AWS depression, the AWS DEM (0.05 m resolution) was subdivided into grids of 3×3 m (9 m^2 , 60×60 pixels), 6×6 m (36 m^2 , 120×120 pixels), 12×12 m (144 m^2 , 240×240 pixels), and 18×18 m (324 m^2 , 360×360 pixels) zones, producing 2082, 586, 147, and 67 individual DEMs, respectively. The gridded approaches were applied to each individual DEM to develop a spatial description of z_0 for each algorithm and direction, spanning a variety of scales.

To estimate z_0 across the entirety of the glacier, the same method was applied to the Lirung DEM (0.25 m resolution), with grid sizes of 6×6 m, 12×12 m, 18×18 m, 24×24 m, 30×30 m, 45×45 m, 60×60 m, 90×90 m, and 120×120 m. Again, the gridded approaches were applied to each individual DEM to develop a spatial description of z_0 for each algorithm and direction, spanning a variety of scales.

Last, the Lirung DEM was coarsened to resolutions of 0.5 m, 1 m, 2 m, and 5 m. Each coarsened DEM was subdivided as for the 0.25 m resolution DEM, and z_0 was calculated for each subdomain using the coarser DEMs.

3.3. Aerodynamic Inversion Approach

Using the tower observations of wind speed and temperature, and applying the profile aerodynamic method based on Monin-Obukhov similarity theory, it is possible to derive the aerodynamic roughness length z_0 and the scalar roughness for temperature $z_{0,T}$.

We derived z_0 and $z_{0,T}$ by optimizing the fit of the tower data to equations (10) and (11), where $u(z)$ and $T(z)$ are wind speed (m s^{-1}) and temperature ($^\circ\text{C}$) at height z , d is the displacement height, u^* and T^* are the friction velocity and scaling temperature, respectively, L is the Monin-Obukhov length ($L = \frac{T(u^*)^2}{kgT^*}$), k is the von Kármán constant (0.4), α_M is assumed to be 0.5, and the Prandtl number Pr is set to 1. With three levels of observation for $u(z)$, the fit of equations (11) and (10) to each profile is determined without iteration but otherwise our analysis followed Sicart *et al.* [2014].

$$u(z) = \frac{u^*}{k} \left(\ln \frac{z+d}{z_0} + \alpha_M \frac{z+d}{L} \right) \quad (10)$$

$$T(z) - T_s = \frac{T^*}{k} \left(Pr \ln \frac{z+d}{z_{0,T}} + \alpha_M \frac{z+d}{L} \right) \quad (11)$$

The validity of this approach depends in part on stability of the surface boundary layer [e.g., Zilitinkevich *et al.*, 2008], and we only analyze profiles for neutral conditions. To quantify stability, we first considered profiles with $u_{2m} \geq 1.5 \text{ m s}^{-1}$ and computed the bulk Richardson number [Moore, 1983; Brock *et al.*, 2010] according to equation (12), where g is the gravitational constant, T_z and T_s are the temperatures at height z and at the surface z_s (K), T_0 is the mean temperature of the air layer (K) and u is the wind speed (m s^{-1}). The parameter z_s is equal to 0 in this case. Following Brock *et al.* [2010] we define near-neutral conditions as $-0.03 < Ri_b < 0.03$.

$$Ri_b = g \frac{T_z - T_s}{T_0 u^2} (z - z_s) \quad (12)$$

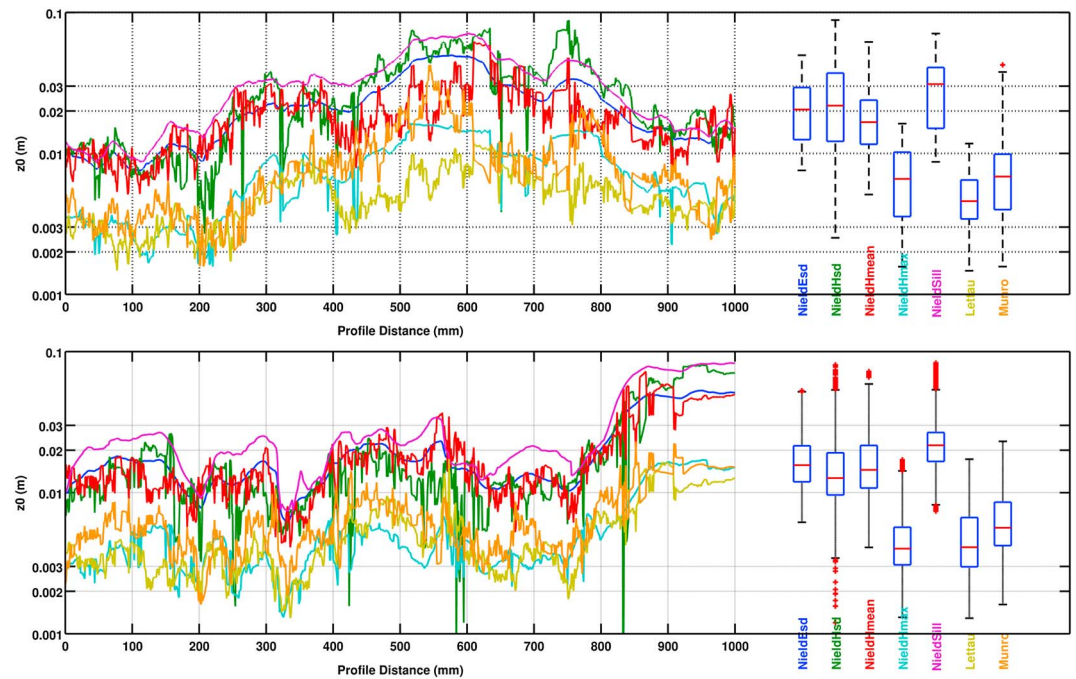


Figure 3. Microtopographic z_0 variability for Plot 5 depending on profile location and method, in (top) cross-glacier and (bottom) down-glacier directions. Each data point corresponds to z_0 estimated from (a) a row or (b) a column of the DEM.

However, the surface boundary layer at our study site rarely satisfies these standard stability criteria: from 483 total half-hourly measurements, only three were obtained with both $u_{2m} \geq 1.5 \text{ m s}^{-1}$ and $|Ri_b| \leq 0.03$. Thus, for this highly heterogeneous surface, derivation of z_0 with standard criteria has a low success rate.

We instead used three different criteria to indicate near-neutral conditions and compared the results to overcome the lack of valid data points. We derived a median value for z_0 from all time steps with (a) $u_{2m} \geq 1.5 \text{ m s}^{-1}$ (u_{2m} criterion), (b) $|Ri_b| \leq 0.03$ (Ri_b criterion), and (c) cloud cover above 70% (cf criterion), which generally supplies more data points. We define the cloud cover as in *Juszek and Pellicciotti [2013]* based on the fraction between measured solar radiation at the nearby AWS and potential clear sky radiation for the time and location computed based on *Iqbal [1983]*, and also require that $u_{2m} \geq 0.5 \text{ m s}^{-1}$.

Finally, we determined the sensitivity of surface roughness derived from wind and temperature data to sensor accuracies following the approach described in *Sicart et al. [2014, Appendix A]*. Since the displacement height d is an unknown but may be substantial on such rugged terrain, it was treated as an additional uncertainty in the equation, and the sensitivity of the results to d was tested for each profile over the range of $|d| \leq 0.1 \text{ m}$ at intervals of 0.002 m.

Table 3. Correlation Slope (b , Below Diagonal) and Strength (R^2 , Above Diagonal) Between Microtopographic Profile Methods for All Plots^a

$b \setminus R^2$	NieldEstd	NieldHstd	NieldHmean	NieldHmax	NieldSill	Lettau	Munro
NieldEstd	\	0.53	0.65	0.67	0.93	0.59	0.62
NieldHstd	0.55	\	0.33	0.82	0.50	0.26	0.30
NieldHmean	0.65	0.60	\	0.55	0.60	0.82	0.13
NieldHmax	2.59	3.74	2.90	\	0.60	0.51	0.38
NieldSill	0.63	0.61	0.63	0.16	\	0.48	0.51
Lettau	2.48	2.15	3.62	0.73	3.39	\	0.27
Munro	2.02	1.84	1.15	0.50	2.79	0.41	\

^a $p < 0.001$ for all comparisons.

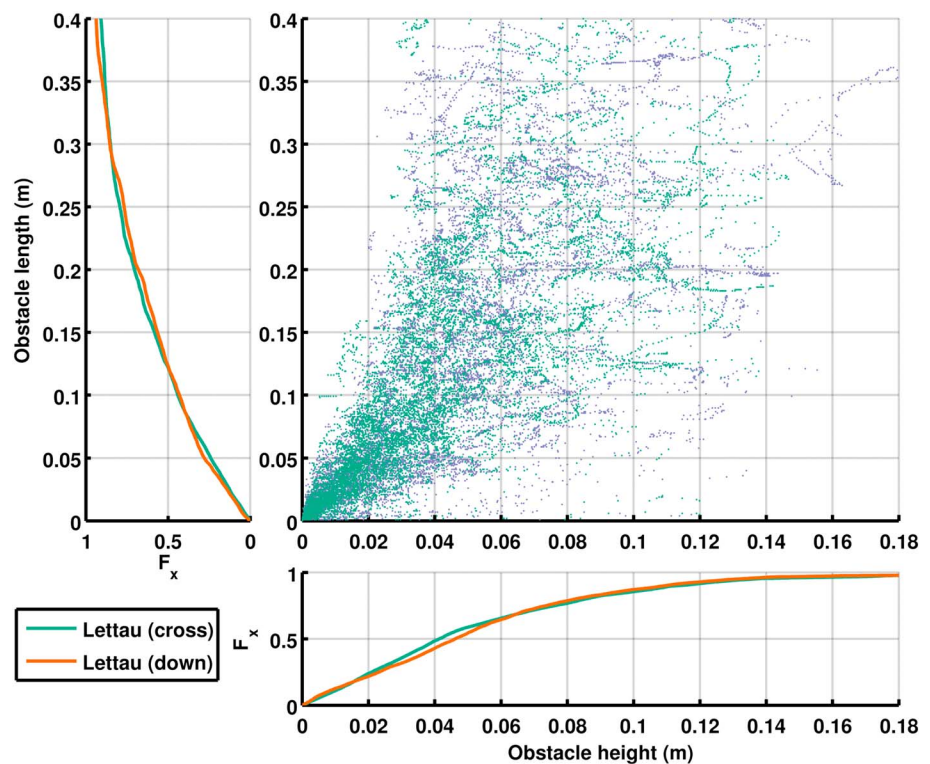


Figure 4. Distribution of obstacle heights and widths determined for Plot 5, demonstrating isotropy for the debris surface. Shown are obstacles determined using Lettau’s zero up-crossing method in the cross-glacier ($n = 6045$) and down-glacier ($n = 6240$) directions, and the empirical cumulative distribution for each.

4. Results

4.1. Microtopographic Plot Transects

The transect-based algorithms produced very different values of z_0 when supplied with the same transect data, consistently spread over an order of magnitude between algorithms (Figure 3). Two distinct groups of values seem to recur across plots and directions: NieldHmax, Lettau, and Munro all estimate $z_0 \sim 0.007$ m, while NieldEstd, NieldHstd, NieldHmean, and NieldSill all produce estimates between 0.015 m and 0.025 m for the 1 m² plots (Table 4). It should be noted that the plots exhibit the smoothest character of surface across the glacier and should represent a lower bound for debris surfaces composed of cobbles and gravel.

However, every algorithm varied by at least 1 order of magnitude between transects of the same plot and direction (Figure 3). The NieldHstd, NieldHmax, Lettau, and Munro algorithms are sensitive to slight changes in the transect topography, resulting in rapid jumps and drops in z_0 and little autocorrelation. The NieldEstd and NieldSill algorithms present smoothly varying and highly autocorrelated sets of z_0 estimates, while the NieldHmean algorithm presents intermediate behavior.

Although they disagree in terms of the magnitude of z_0 , all the estimates vary in roughly the same manner between transects in response to topographic changes (Figure 3). Directly comparing all estimates from the

Table 4. Mean z_0 Estimate for Each Microtopographic Method in Cross-Glacier and Down-Glacier Profiles at Each Plot

	NieldEstd		NieldHstd		NieldHmean		NieldHmax		NieldSill		Lettau		Munro	
	Cross	Down	Cross	Down	Cross	Down	Cross	Down	Cross	Down	Cross	Down	Cross	Down
Plot 1	0.0165	0.0166	0.0139	0.0144	0.0175	0.0192	0.0045	0.0049	0.0200	0.0181	0.0048	0.0058	0.0056	0.0058
Plot 2	0.0214	0.0189	0.0190	0.0179	0.0234	0.0204	0.0059	0.0056	0.0274	0.0263	0.0060	0.0053	0.0064	0.0059
Plot 3	0.0165	0.0111	0.0188	0.0108	0.0153	0.0106	0.0056	0.0031	0.0181	0.0158	0.0039	0.0024	0.0060	0.0033
Plot 4	0.0169	0.0206	0.0159	0.0174	0.0202	0.0226	0.0053	0.0060	0.0193	0.0260	0.0062	0.0074	0.0059	0.0079
Plot 5	0.0223	0.0204	0.0218	0.0207	0.0192	0.0220	0.0062	0.0058	0.0309	0.0296	0.0051	0.0059	0.0085	0.0066

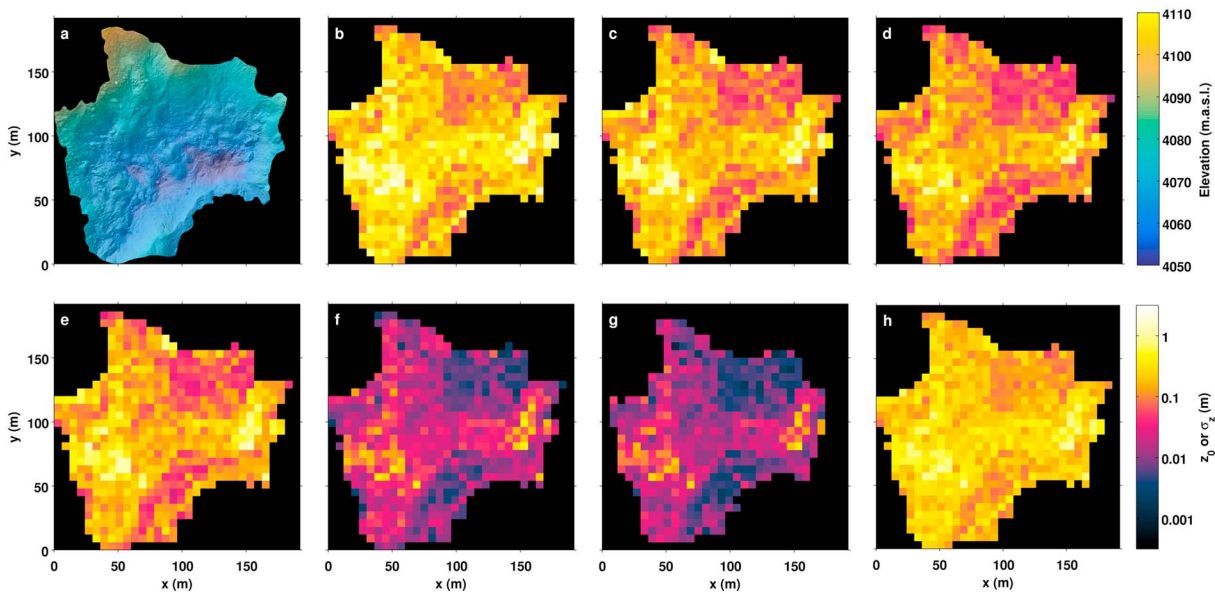


Figure 5. Variability of z_0 for the AWS depression, showing (a) the study depression elevation and hillshade and z_0 grid-based estimates from (b) NieldEstd, (c) NieldHStd, (d) NieldHmean, (e) NieldHmax, (f) Lettau, and (g) Munro methods, also showing (h) the subgrid standard deviation of elevation σ_z . Results are for 6 m grids.

five plots, all algorithms are strongly correlated to each other (Table 3), with $p < 0.001$ for all comparisons and correlation R^2 values ranging from 0.13 (NieldHmean and Munro) to 0.93 (NieldEstd and NieldSill).

The plots exhibit isotropic elevation variability due to the very similar populations of obstacles determined for each direction of analysis (Figure 4). The z_0 estimates determined in cross-glacier and down-glacier directions are in very close agreement for each algorithm and plot (Table 4), and these directional values are very rarely more than 20% different.

In spite of the strong variability between algorithms and transects, the plots show a fairly consistent pattern of z_0 estimates for each algorithm and direction (Table 4). With few exceptions, Plots 2, 4, and 5 produced higher values of z_0 , while lower z_0 values were estimated for Plots 1 and 3.

4.2. Microtopographic Grids for the AWS Depression

The values of z_0 estimated for the AWS DEM differed based on algorithm and grid size. As with the transect results, the Munro and Lettau estimates of z_0 were an order of magnitude lower than those from the Nield

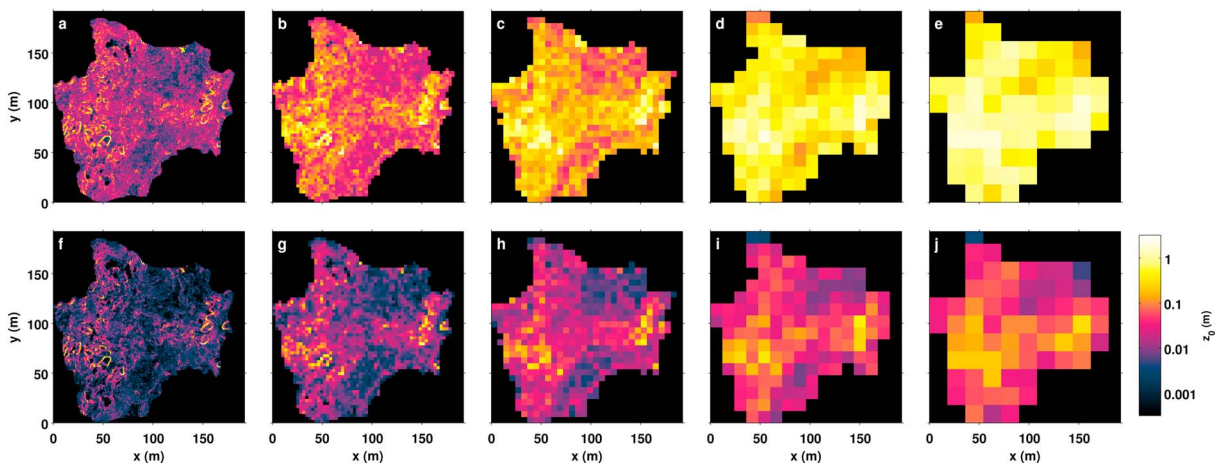


Figure 6. Scale-dependent results for the AWS depression, showing results from the (a–e) NieldEstd and (f–j) Lettau algorithms at the 1 m (Figures 6a and 6f), 3 m (Figures 6b and 6g), 6 m (Figures 6c and 6h), 12 m (Figures 6d and 6i), and 18 m (Figures 6e and 6j) grid scales. Values tend toward the maximum value within the zone at smaller scales.

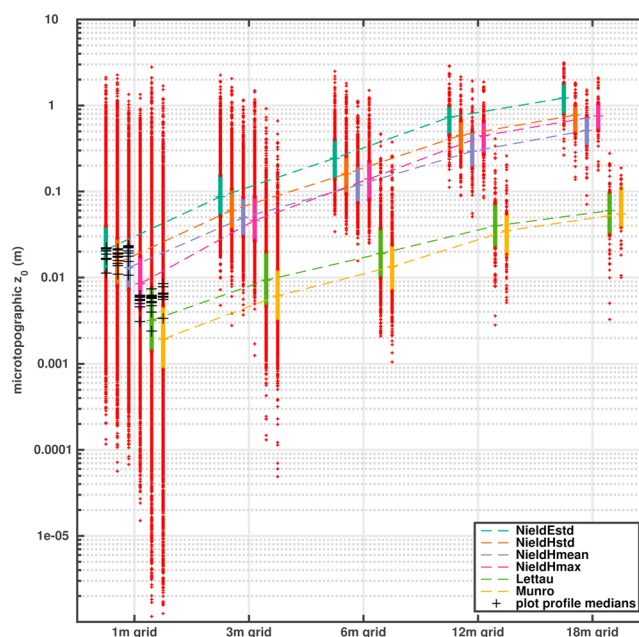


Figure 7. Scale dependence of microtopographic z_0 estimates for the AWS DEM, with median values of z_0 increasing by more than an order of magnitude over the scales analyzed, and results from the larger scale dominated by high-roughness outliers from the smaller scales. Also plotted are the mean profile-based results for each algorithm from the 1 m² plots, which correspond closely to the values from the 1 m gridded AWS DEM in spite of 50× resolution difference.

empirical models (Figure 5). However, each algorithm produced a similar range of values (2 orders of magnitude) and reproduced a common spatial pattern of high and low z_0 estimates. High values of z_0 (0.5 to 5 m, depending on the algorithm) correspond to high-relief areas composed of large boulders, while lower estimates (0.005 to 0.05 m) are produced for more homogeneous cobbled areas. This spatial pattern is also exhibited by the subgrid standard deviation of detrended elevations (σ_z), suggesting a direct link between grain size, packing, and aerodynamic roughness length [Evatt *et al.*, 2015].

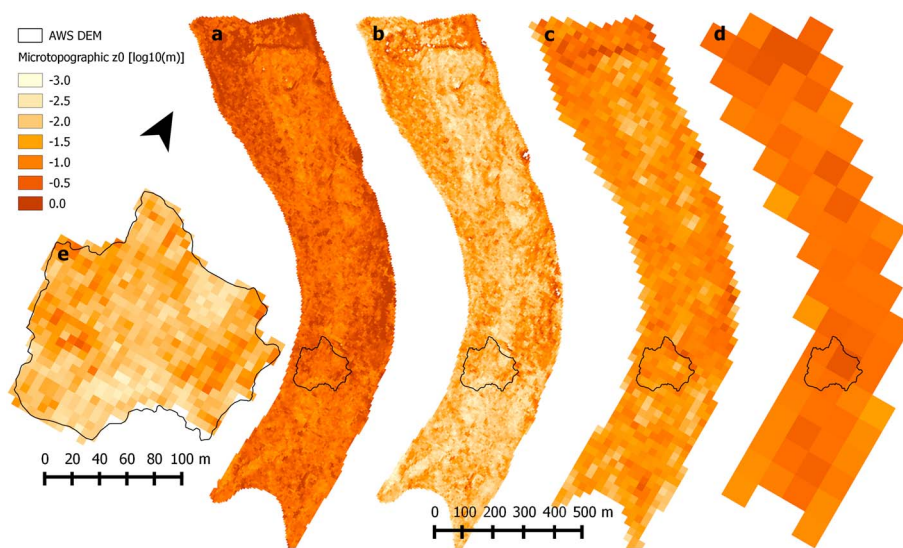


Figure 8. Spatial variability and scale dependence of microtopographic z_0 estimates for the Lirung DEM, showing (a) NieldHstd and (b) Lettau results for the 6 m grid scale, as well as Lettau results for (c) 24 m and (d) 90 m grid scales. (e) Inset shows the Lettau 6 m grid results for the AWS DEM area. All results are derived from the Lirung DEM with 0.25 m resolution. Displayed values are $\log_{10}z_0$.

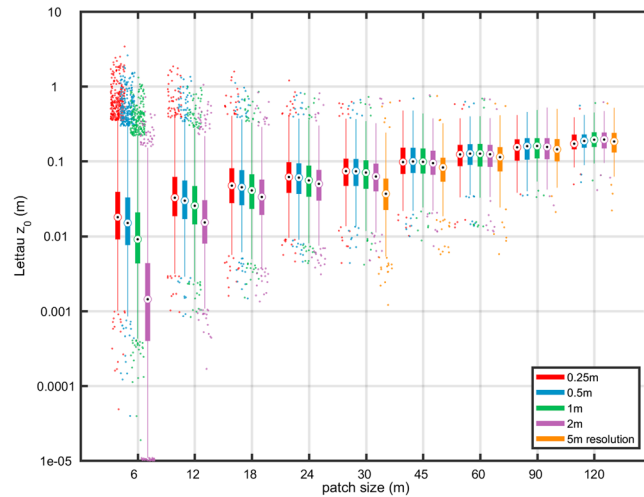


Figure 9. Scale and resolution dependence of microtopographic z_0 estimates for the Lirung DEM (shown for the Lettau method). Increasing grid size results in increased estimates of z_0 regardless of resolution differences for all methods. Coarser DEMs produce low z_0 estimates when the grid encompasses less than 100 pixels (10×10).

Unfortunately, all the models show a strong dependence of z_0 on the grid size analyzed. As the grid size is enlarged, estimates tend toward the highest value within the subdomain at finer scales, but similar spatial patterns are produced by each grid scale and algorithm (Figure 6, showing results for the NieldEstd and Lettau algorithms). This scale dependence is apparent for all algorithms in Figure 7a. The 1 m grids produce values in close agreement with the study plots in spite of a very large resolution difference (0.001 m versus 0.05 m). However, the algorithms produce higher values for larger grids, although they have the same spatial resolution (0.05 m).

4.3. Microtopographic Grids for the Whole Glacier

The values of z_0 estimated for the Lirung DEM at 0.25 m resolution again differed based on algorithm and grid size. The Munro and Lettau estimates of z_0 were again an order of magnitude lower than the Nield estimates, but the algorithms reproduced similar patterns of z_0 . As with the AWS depression, all the algorithms show a strong dependence of z_0 on the grid size, with increasing z_0 estimates for any resolution (Figures 8 and 9, showing results for the Lettau algorithm). Differences in grid resolution, however, have a limited effect on microtopographic z_0 (Figure 9). For any grid size, DEM resolutions that result in $\sim 10 \times 10$ pixels or more produce very similar results, while undersampling is problematic for relatively coarser grids (Figure 9).

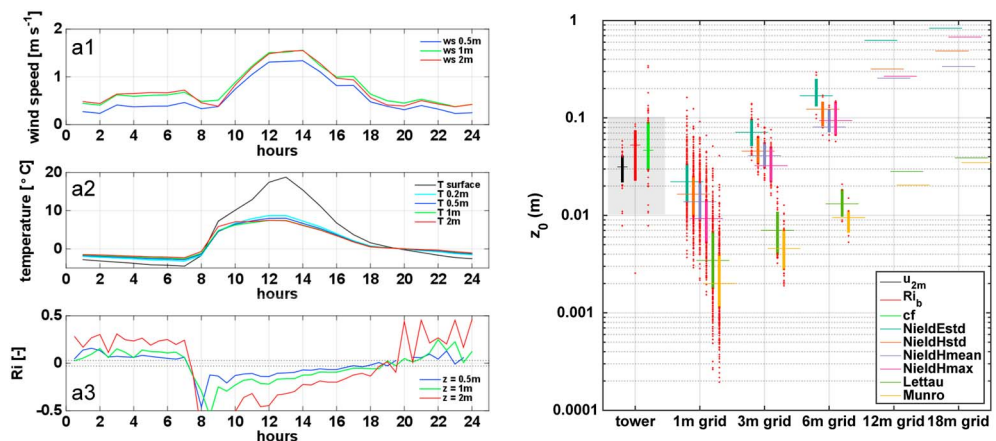


Figure 10. (a1) Diurnal cycle of wind speed, (a2) temperature, and (a3) the Richardson number for the study period (11 days). The black dotted lines mark the absolute value of 0.03 for Ri_b , a threshold used by [Brock et al., 2010] for near-neutral conditions. Aerodynamic z_0 derived at the tower for different criteria and microtopographic z_0 derived from the DEM with different methods in an area of 18×18 m around the wind tower (12×12 m for the 12 m resolution DEM). The grey area marks the range of possible uncertainty of the overall z_0 results from tower data.

Table 5. Median Values and Standard Deviations for z_0 Based On Different Stability Criteria, Indicating the Number of Profiles Satisfying Each Criterion (n)^a

Criterion (n)	Median z_0 (m)	σ (m)	Range z_0 (m)	Sensitivity to d (m/m)
u_{2m} (42)	0.03	0.01	0.01–0.14	0.28
Ri_b (8)	0.05	0.03	0.02–0.13	0.21
cf (63)	0.05	0.06	0.02–0.13	0.30

^aAlso shown are the uncertainty range considering sensor uncertainties (Range z_0), and the sensitivity of z_0 to displacement height d .

4.4. Wind Tower z_0 Inversion

The u_{2m} criterion is only met when wind is blowing down-glacier along smoother surfaces (unobstructed by large hummocks) below and above the towers. Wind measurements carried out with individual sensors at different locations of the debris surface and measurements from 2 AWS locations confirm that such low mean wind speeds are common for the entire debris-covered area, but with considerable differences between depressions and debris mounds during the day (not shown). From 483 total half-hourly observation sets, only 42 satisfy $u_{2m} \geq 1.5 \text{ m s}^{-1}$ and provide a median value for z_0 of 0.03 m with a standard deviation of 0.01 (Figure 10). Only eight observation sets satisfy the Ri_b criterion, resulting in a median z_0 of 0.05 m and a standard deviation of 0.03 m. Sixty-three observation sets met the cf criterion, resulting in z_0 of 0.05 m with a larger standard deviation of 0.06.

Considering uncertainties in all wind sensors, the value for z_0 lies between 0.01 m and 0.14 m (Table 5). This range is similar to the findings of *Sicart et al.* [2014] for clean ice on a logarithmic scale, but with larger absolute values. Additionally, the unknown displacement height could result in a further change of z_0 by up to ± 0.03 m, assuming a possible displacement height of ± 0.1 m for the location of the tower (Table 5).

Considering the few wind profiles with $u_{2m} \geq 1.5 \text{ m s}^{-1}$ and $|Ri_b| \leq 0.03$, we can derive only three valid values for z_{0r} (0.015, 0.005, and 0.001), which on average is in accordance with earlier measurements and theory [*Andreas, 1987; King and Anderson, 1994; Calanca, 2001*], but the data are insufficient to make a definite statement on an actual value of z_{0r} over debris.

5. Discussion

5.1. Scales of Surface Roughness and the Roughness Sublayer

All of the microtopographic algorithms exhibit a sensitivity to profile length (Figure 6). Lettau's algorithm was intended to be independent of length [*Lettau, 1969*] but increases with increasing grid size (Figure 8). *Munro* [1989] analyzed 20 m \times 20 m grids posted at 0.5 m and 1 m spacing, and *Brock et al.* [2006] found that the z_0 estimated by the Munro algorithm was independent of scale for profiles of 3 to 15 m. However, the Munro algorithm was specifically intended to emulate the Lettau results, which it accomplishes for our study site at all scales, and thus it shows the same scale dependence, including those for the 3 to 15 m profile lengths.

Rounce et al. [2015] found that Munro underestimates z_0 for small plots of 1 m² or 4 m², and our results agree with that finding, in spite of uncertainty with the wind tower data. This could be, in part, because plots were smaller in scale than is suitable for the method, although reasonable values were found by *Irvine-Fynn et al.* [2014] for small grids. *Smeets et al.* [1999] suggest that such a consistent difference could be explained by the fact that the original formula by *Lettau* [1969] was derived for cubes in a wind tunnel, which have a larger silhouette area than more streamlined objects such as boulders or ice surfaces. More importantly, the very small plots may not include a large enough obstacle population to represent the glacier surface.

Scale dependence is inherent within the algorithms: the Lettau and Munro algorithms explicitly include transect length X as a term, and the metrics on which the Nield empirical approaches are based ($\sigma_z, H_\sigma, H_{\text{mean}}, H_{\text{max}}$) also increase with length. This is, in part, because linear detrending (planar fit) does a poorer job removing large undulations as length increases. Thus, as length increases, so do $\sigma_z, H_\sigma, H_{\text{mean}}, H_{\text{max}}$. This problem could be reduced by application of more sophisticated detrending methods (e.g., polynomial, spline, or median filter), but requires evaluation of the physically meaningful partition scale for near-surface meteorology [*Smith, 2014*].

To circumvent the scale issue, *Rees and Arnold* [2006] recommended elevation transects <0.1 m in length at millimeter sampling intervals or a few meters in length at centimeter intervals, matching the scale-independent range identified by *Brock et al.* [2006]. The 6–18 m grids for the AWS depression meet this latter profile recommendation, and at these scale the Lettau and Munro algorithms produce estimates generally in line with the literature (Table 1), with quartile values of 0.008 m to 0.08 m, and in general agreement with the range of values determined at the plots and for the tower.

For Lirung Glacier, the standard deviation of detrended elevations increases with range up to at least 120 m. This pattern could eventually stabilize with a larger grid size (several hundred meters) encompassing many such depressions to describe a characteristic topographic roughness for this type of surface. However, while large ridges (~ 20 m) with an interridge spacing of ~ 200 m may be crucial for atmospheric shear across a heavily downwasted debris-covered glacier, the semilogarithmic wind profile of Monin-Obukhov similarity theory occasionally holds true even within the depression. This suggests that the large-scale characteristic roughness is greater in extent than is important for surface energy balance considerations within the depression, and that the physically meaningful topographic partition scale for this type of roughness is within the range of scales investigated.

This closely fits the dense-obstacle theory of [*Brutsaert*, 1992] as applied to a very rough glacier surface by *Smeets and van den Broeke* [2008a], whereby the large hummocks dominate the overall drag of the surface to drive development of a semilogarithmic inertial sublayer. Beneath this lies an intermediate roughness sublayer (RSL), which is very heterogeneous, and underlain by a viscous sublayer. Importantly, the surface transfer of energy within the underlying viscous sublayer is driven by microscale roughness elements rather than those at the larger scale. We have higher confidence in extraction of these obstacles from the smaller grids, as the linear detrending removes sufficient background variability. At the 3 and 6 m scales, the z_0 estimates generally fit the values derived from the wind tower (0.03–0.05 m), and are higher than most reported values (Table 1). Accordingly, results from the Nield algorithms suggest that z_0 varies across Lirung Glacier between ~ 0.005 m (smooth cobbles) and ~ 0.5 m (large boulders).

5.2. Evaluation of Microtopographic z_0 Algorithms and Comparison to Aerodynamic Estimate

In spite of the differences between the mechanistic (Lettau, Munro) and empirical (Nield) algorithms, nearly all algorithms correlated to one another for a given transect length and sampling interval (Table 3), reproducing similar spatial patterns across the study area (Figure 5). This gives strong confidence that each approach provides some proxy of roughness, although the spread of values reduces confidence in the estimates' magnitude.

Lettau and Munro results are in close agreement with each other, but are typically one fourth or less of the Nield empirical model values for the plots and for the grids, regardless of scale of analysis. Although these methods have been used and validated for clean ice glacier surfaces (Table 1), values in prior studies have generally been less than 0.005 m. Prior microtopographic investigations of debris-covered surfaces have also suggested that the Munro method produces values of z_0 lower than expected relative to aerodynamic values [*Rounce et al.*, 2015], although this could be partly due to the scale analyzed. *Nield et al.* [2013b] established empirical relationships for a range of surface types (z_0 from 8×10^{-5} m to ~ 0.04 m), and the results from our tower location (~ 0.01 – 0.14 m) is in the same range, giving some confidence of the magnitude of values produced by these algorithms.

It is encouraging that with each of the three stability criteria (u_{2m} , Ri_b , and cf), we reach similar median values for z_0 between 0.03 and 0.05 m. While these values are larger than those found by *Brock et al.* [2010] at Miage Glacier (0.016 m), the hummocky topography of Lirung Glacier would suggest a higher value of z_0 . However, taking uncertainties of sensors, unknown displacement height, and potentially strong local variations of surface temperature into account, these values should not be considered definite results. Rather, the measurements from the tower support an order-of-magnitude range: $z_0 \sim 0.01$ – 0.1 m. Longer micrometeorological data sets for multiple sites would be necessary to confirm the validity of the underlying similarity theory used to derive these results and constrain the margin of uncertainty. Certainly, tower location selection is important: at our site, finding a location on glacier with a consistent fetch longer than 50 m in the dominant wind direction was not possible. The chosen location is instead representative of the very hummocky terrain of debris-covered glaciers in the catchment, but proved a challenge for determination of z_0 from 2 m wind and temperature profiles.

To compare the z_0 estimates obtained from meteorological and microtopographic methods, we collected the values derived by the microtopographic approach for the different resolutions at the tower location in the 18×18 m area surrounding the tower (12×12 m for the 12 m grid) (Figure 10). This zone may not correspond directly to the footprint that leads to the measured aerodynamic roughness at the tower (this may be a much longer fetch in line with the dominant wind) but gives an indication as to which combinations of method and grid size are of a comparable magnitude to the tower results. Estimates of microtopographic roughness at the location of the AWS agree with the value derived from tower data (0.01–0.1 m) for the Nield algorithms at grid sizes ≤ 3 m (Figure 10). For reasons discussed above, z_0 values increase with scale, and at grid scales 12–18 m it is the Lettau and Munro methods that provide values in closer agreement with atmospheric data, although they may do so for the wrong reasons (i.e., their estimates are not based on the microscale roughness elements).

With lower confidence in the magnitude of the Lettau and Munro algorithms for debris-covered glaciers [Rounce *et al.*, 2015], and lacking a mechanistic microtopographic model for z_0 that has been extensively validated at a wide range of scales, it is noteworthy that estimates of z_0 correlate to more direct measures of elevation variability [Nield *et al.*, 2013b]. For example, high-resolution maps of σ_z within a window (e.g., Figure 6j or Rippin *et al.* [2015]) may be considered a good proxy for z_0 variability, as it is easy to measure. To make use of σ_z in estimating z_0 , a DEM is needed at high enough resolution to resolve the small height differences controlling energy transfer in the viscous sublayer for very hummocky topography [Smeets and van den Broeke, 2008a], and it is clearly necessary to define the topographic partition scale in order to analyze the microtopographic variations.

In spite of the challenges, these results are encouraging for future studies as measuring aerodynamic roughness lengths for debris-covered glaciers facies is very difficult. Thick debris cover heats up considerably during the day, causing the near-surface temperature profile to invert [Brock *et al.*, 2010; Steiner and Pellicciotti, 2016]. The surface on such glaciers can be very hummocky and does not allow for long fetches of uniform topography, a normal requirement for this type of analysis (usually 50 m or more). For Lirung Glacier, very little of the study basin would actually meet this observational requirement. Consequently, a measurement bias toward “smoother” and more uniform surface due to the requirement of a large homogeneous fetch [Wiernga, 1993] is probable for the few studies using aerodynamic inversion to measure z_0 for these surfaces (Table 1).

5.3. Variability of z_0 for a Debris-Covered Glacier

The results of this study indicate that z_0 is a highly variable surface characteristic for debris-covered glaciers. While distinct values of z_0 were produced by different algorithms and for different grid sizes, the underlying spatial variations in roughness estimates are common across algorithms and grid sizes. The z_0 varies by at least 2 orders of magnitude across the AWS DEM and 3 orders of magnitude across the Lirung DEM. At the plot scale, the algorithms are strongly correlated (Table 3), although they differ in magnitude and sensitivity to precise transect location (Figure 3). Even at this very fine scale, results from any algorithm span an order of magnitude. Part of the spatial variability may be attributed to differences in microtopographic algorithms and their sensitivity to DEM detrending and transect length. The consistent 4 \times difference between the mechanistic (Lettau/Munro) and empirical (Nield) algorithms increases uncertainty in z_0 , but the two families of algorithms reproduce the same spatial variations within plots and across the entire study area.

Spatial variations in aerodynamic roughness length are common for clean ice glaciers between surface facies [Brock *et al.*, 2006; Smeets and van den Broeke, 2008b; Rippin *et al.*, 2015]. For a debris-covered glacier, spatial variability of z_0 is linked to grain size and packing [Evatt *et al.*, 2015]. This is implicit in the mechanistic and empirical z_0 algorithms, and our analysis indeed produces the highest values of roughness near large boulders and heterogeneous surfaces (~ 0.5 m). Conversely, lower values of z_0 (~ 0.01 m) occur for homogeneous zones of cobbles in the area of the AWS.

It is important to note that z_0 is also not constant in time for glacier surfaces [Smeets *et al.*, 1999; Smeets and van den Broeke, 2008b; Nield *et al.*, 2013a], for example, varying seasonally due to snow metamorphism. Although this mechanism is less important for debris-covered glaciers during the ablation season, temporal variations in z_0 may occur due to episodic snowfall or debris remobilization and sorting. Additionally, our aerodynamic inversion results vary diurnally by 1 order of magnitude, as estimated z_0 depends on wind speed, which determines the surface viscous layer development.

5.4. Implications for Energy-Balance Modeling

Values of z_0 used by surface energy balance modeling studies for debris-covered glaciers are very limited in range, with most values fixed spatially and falling in the range 0.01 to 0.016 m (Table 2). These values may be characteristic for some debris-covered glacier surfaces, but such glaciers vary greatly in surface composition [Janke *et al.*, 2015]. Many exhibit high-relief surface depressions similar to our study site [Iwata *et al.*, 1980; Thompson *et al.*, 2016], and it is probable that literature values are biased to smaller values of z_0 due to observational requirements. It is also clear that a single fixed value is a poor representation for sites exhibiting variable grain sizes [Inoue and Yoshida, 1980; Rounce *et al.*, 2015].

Determining representative z_0 values for surfaces of differing character is important, because uncertainties and spatial variations in z_0 may be extremely important for model error in melt calculations [Fausto *et al.*, 2016]. Rounce *et al.* [2015] found a moderate sensitivity of the net surface energy balance to z_0 parameter choice and found higher model sensitivities to z_0 for thicker debris. Modeling debris thickness with an inversion of the energy balance, Foster *et al.* [2012] find the results to be very sensitive to z_0 . Based on the values obtained across the AWS DEM, we suggest that surface energy balance models test sensitivity to a broad range of values, as z_0 can vary from 0.005 to 0.5 m across the range of surface conditions encountered at a heterogeneous debris surface (values from 6 m grid scale). Studies of individual sites, however, may be able to narrow the range simply by taking into account the surface composition, such as gravel ($z_0 \lesssim 0.01$ m), cobbles (~ 0.01 – 0.05 m), or boulders ($\gtrsim 0.05$ m), and smooth ($\lesssim 0.02$ m) or hummocky ($\gtrsim 0.05$ m) character.

It is clear that a single value of z_0 poorly represents the surface conditions of a hummocky debris-covered glacier. Considering the high spatial variability of turbulent fluxes across glacier surfaces [Sauter and Galos, 2016], aerodynamic roughness length variations may certainly play a strong role in determining the net surface energy balance, but this is yet to be determined.

Constraining turbulent energy transfer for a hummocky debris-covered glacier is extremely difficult for even a single location. In addition to the heat-regulating effect of the debris surface [Evatt *et al.*, 2015], the hummocky character of heavily downwasted debris-covered glaciers greatly complicates application of Monin-Obukhov theory. Rather, the large hummocks and hollows interact to produce an unstable and heterogeneous roughness layer [Shao and Yang, 2008], while turbulent energy transfer to the surface may be constrained by the underlying viscous sublayer controlled by roughness elements at the microtopographic scale [Smeets and van den Broeke, 2008a]. Thus, for this type of surface, aerodynamic inversion of wind tower data has a low success rate, as the sensors generally occupy the unstable roughness layer.

6. Conclusions

This study used SfM surveys at plot (1 m²), local (21,300 m²), and glacier (550,000 m²) scales to create high-resolution DEMs (1 mm, 0.05 m, and 0.25 m, respectively) for a hummocky debris-covered glacier, and applied a variety of microtopographic methods to estimate z_0 and compared the results to values obtained by aerodynamic inversion of wind tower data. We find that z_0 is highly variable across the debris-covered surface, varying by 2 orders of magnitude within the study area.

At the plot scale, we find that algorithms are sensitive to small profile differences. Within a single small plot (1 m², 0.001 m resolution), each algorithm produced estimates varying by at least a factor of 10, although variability at this scale is probably not meaningful for turbulent energy transfer. Estimates of z_0 from cross-glacier and down-glacier profiles are similar for any algorithm, unlike anisotropic bare-ice surfaces. Results from the mechanistic and empirical microtopographic algorithms are strongly correlated to one another, but differ greatly in magnitude. A gridded method aggregating all possible transects is more representative, as z_0 is isotropic for the debris surface.

For the AWS depression, the gridded empirical methods (NieldEstd, NieldHstd, NieldHmean, and NieldHmax) closely matched the plot-derived and aerodynamically derived values if a grid size of 1 m or 3 m was used (0.05 m resolution), while the mechanistic methods (Lettau, Munro) produced estimates of the correct magnitude for a grid size of 12–18 m. However, microtopographic methods of z_0 estimation all have a strong dependence on scale of analysis, increasing continuously as the transect length increased. Thus, the topographic partition scale for z_0 presents a challenge for distributed estimation of z_0 , and is a priority for future research. Although algorithms disagree in magnitude, we suggest a range of z_0 encompassing 0.005 to 0.5 m to represent the surface conditions encountered at a heterogeneous debris surface. Energy-balance

modeling efforts, however, may be able to narrow the range by considering the surface composition, such as gravel ($z_0 \lesssim 0.01$ m), cobbles (~ 0.01 – 0.05 m), or boulders ($\gtrsim 0.05$ m), and smooth ($\lesssim 0.02$ m) hummocky ($\gtrsim 0.05$ m) character. It is clear, though, that z_0 is highly variable across the glacier surface, regardless of the partition scale chosen.

At our study site, z_0 determined from wind tower observations ranges between 0.01 and 0.1 m, with median values ranging between 0.03 and 0.05 m for different stability criteria representing near-neutral conditions. The larger range of uncertainty is due to sensor accuracy as well as the unknown displacement height, which may be substantial. These are generally higher values than have been observed for debris-covered glaciers or than has been tested in energy balance models. Our study site may exhibit higher-relief than other measurement locations, but is fairly typical for a downwasting heavily debris-covered glacier. Site selection is important for use of aerodynamic inversion methods (leading to fewer successful measurements of z_0 at our site), but may bias similar studies to low-roughness locations.

It can be questioned whether this aerodynamic approach, using similarity theory, is suitable to determine z_0 for such complex topography. *Liang et al.* [2014] show that the Monin-Obukhov similarity theory may not be valid when $u_{2m} \leq 1$ m s⁻¹ for $Ri_b \leq 0.3$, and $u_{2m} \leq 1.5$ m s⁻¹ for $Ri_b > 0.3$ (Regime 3). The longer record of measurements at our AWS indicate that conditions are often close to these thresholds. As a dominant behavior for this type of surface, it is important to understand near-surface dynamics in this regime. Alternative means to determine surface roughness at the point scale would be to measure turbulent fluxes directly with an eddy covariance system or invert an energy balance and derive z_0 as a residual. The latter approach needs to first ensure that other inherent uncertainties in the energy balance can be reduced relative to uncertainty in the value of z_0 itself.

In light of the difference between empirical and mechanistic z_0 estimates, and the difficulty in measuring the aerodynamic roughness length from meteorological data (for high-relief hummocky terrain such as the study site), we suggest that studies maintain a clear distinction between *microtopographic* and *aerodynamic* roughness. Mechanistic microtopographic models [e.g., *Lettau*, 1969; *Counihan*, 1971; *Munro*, 1989] measure topographic roughness and attempt to link this property to the aerodynamic roughness length [*Smith*, 2014], but still require validation across a wider range of surface types. While such models are thoroughly established for many glacier surfaces [*Brock et al.*, 2006; *Smith et al.*, 2015a] and may be accurate for smoother debris surfaces as well [*Quincey et al.*, 2017], validation data for hummocky topography is difficult to assemble. Thus, while a mechanistic model of z_0 based on surface drag is appealing, empirical parameterizations of z_0 [*Nield et al.*, 2013b] may still be more reliable models to relate the two types of roughness. In either case, a high-resolution (few centimeters) DEM is needed to assess the variability of z_0 across the glacier surface.

Our results highlight the following opportunities for future study. First, considering the range of values encountered across the study site, surface energy balance model optimization for debris-covered glaciers should consider a range of 0.005 to 0.5 m to account for the surface types commonly found on debris-covered glaciers. This range can be narrowed based on the grain size distribution and relief of a given study site, but order-of-magnitude variability occurs for any algorithm, and these results have high uncertainty due to their scale dependence. Such differences in z_0 can have strong implications for glacier melt [*Fausto et al.*, 2016; *Sauter and Galos*, 2016].

Second, novel research is needed to characterize z_0 for hummocky terrain in order to understand the transfer of energy between the semilogarithmic, roughness, and viscous sublayers [*Smeets and van den Broeke*, 2008a]. To accomplish this would require distributed measurements of wind combined with high-resolution topographic observation and modeling (a LES) [e.g., *Sauter and Galos*, 2016]. A key output would be determination of the physically meaningful topographic partition scale for turbulent fluxes [*Smith*, 2014], which would represent a significant advance in understanding boundary layers generally, and especially for these highly heterogeneous landscapes.

References

- Andreas, E. L. (1987), A theory for the scalar roughness and the scalar transfer coefficients over snow and sea ice, *Boundary Layer Meteorol.*, 38, 159–184.
- Azam, M. F., P. Wagnon, C. Vincent, A. L. Ramanathan, V. Favier, A. Mandal, and J. G. Pottakkal (2014), Processes governing the mass balance of Chhota Shigri Glacier (western Himalaya, India) assessed by point-scale surface energy balance measurements, *Cryosphere*, 8(6), 2195–2217, doi:10.5194/tc-8-2195-2014.

Acknowledgments

We would like to thank Tek Rai and his team for help in the field as well as Pascal Buri and Francesca Pellicciotti for assistance with meteorological measurements. We are indebted to Haijing Wang for assistance in translating the *Wang et al.* [2014] manuscript. We are also grateful to numerous people from cryospheric and atmospheric science disciplines who discussed this topic with us at AGU 2015 and EGU 2016. Finally, we would like to thank our Editor Minghua Zhang and three anonymous reviewers, whose insights and suggestions have greatly improved the manuscript. All meteorological and elevation data are available via Mendeleev Data [http://dx.doi.org/10.17632/m2g3mg4364.1 *Miles et al.*, 2017a]; any additional data may be obtained from ES Miles (e.s.miles@leeds.ac.uk).

- Brock, B., A. Rivera, G. Casassa, F. Bown, and C. Acuña (2007), The surface energy balance of an active ice-covered volcano: Villarrica Volcano, southern Chile, *Ann. Glaciol.*, *45*(1), 104–114, doi:10.3189/172756407782282372.
- Brock, B. W., I. C. Willis, and M. J. Sharp (2006), Measurement and parameterization of aerodynamic roughness length variations at Haut Glacier d'Arolla, Switzerland, *J. Glaciol.*, *52*(177), 281–297, doi:10.3189/172756506781828746.
- Brock, B. W., C. Mihalcea, M. P. Kirkbride, G. Diolaiuti, M. E. J. Cutler, and C. Smiraglia (2010), Meteorology and surface energy fluxes in the 2005–2007 ablation seasons at the Miage debris-covered glacier, Mont Blanc Massif, Italian Alps, *J. Geophys. Res.*, *115*, D09106, doi:10.1029/2009JD013224.
- Brun, F. (2015), Monitoring supra-glacial ice-cliffs over debris-covered glaciers using high resolution ground measurements, Master's thesis, Université Joseph Fourier, Grenoble, France.
- Brun, F., et al. (2016), Quantifying volume loss from ice cliffs on debris-covered glaciers using high resolution terrestrial and aerial photogrammetry, *J. Glaciol.*, *62*(234), 684–695, doi:10.1017/jog.2016.54.
- Brutsaert, W. (1992), Stability correction functions for the mean wind speed and temperature in the unstable surface layer, *Geophys. Res. Lett.*, *19*(5), 469–472, doi:10.1029/92GL00084.
- Calanca, P. (2001), A note on the roughness length for temperature over melting snow and ice, *Q. J. R. Meteorol. Soc.*, *127*(571), 255–260, doi:10.1002/qj.49712757114.
- Chappel, A., and G. L. Heritage (2007), Using illumination and shadow to model aerodynamic resistance and flow separation: An isotropic study, *Atmos. Environ.*, *41*, 5817–5830, doi:10.1016/j.atmosenv.2007.03.037.
- Collier, E., L. I. Nicholson, B. W. Brock, F. Maussion, R. Essery, and A. B. G. Bush (2014), Representing moisture fluxes and phase changes in glacier debris cover using a reservoir approach, *Cryosphere*, *8*(4), 1429–1444, doi:10.5194/tc-8-1429-2014.
- Collier, E., L. I. Maussion, F. Nicholson, T. Mölg, W. W. Immerzeel, and A. B. G. Bush (2015), Impact of debris cover on glacier ablation and atmosphere–glacier feedbacks in the Karakoram, *Cryosphere*, *9*(4), 1617–1632, doi:10.5194/tc-9-1617-2015.
- Counihan, J. (1971), Wind tunnel determination of the roughness length as a function of the three-dimensional roughness elements, *Atmos. Environ.*, *5*, 637–642.
- Dabski, M. (2012), Determining rock surface micro roughness and search for new method of relative dating of glacial landforms; a case study from Fláajökull (SE Iceland) and Biferten glacier, *Landform Anal.*, *21*, 3–8.
- Dong, Z., X. Liu, and X. Wang (2002), Aerodynamic roughness of gravel surfaces, *Geomorphology*, *43*(1–2), 17–31, doi:10.1016/S0169-555X(01)00097-6.
- Evatt, G. W., I. D. Abrahams, M. Heil, J. Kingslake, S. L. Mitchell, C. Andrew, and C. D. Clark (2015), Glacial melt under a porous debris layer, *J. Glaciol.*, *61*(229), 825–836, doi:10.3189/2015JoG14J235.
- Fausto, R. S., D. van As, J. E. Box, W. Colgan, P. L. Langen, and R. H. Mottram (2016), The implication of nonradiative energy fluxes dominating Greenland ice sheet exceptional ablation area surface melt in 2012, *Geophys. Res. Lett.*, *43*, 2649–2658, doi:10.1002/2016GL067720.
- Foster, L. A., B. W. Brock, M. E. J. Cutler, and F. Diotri (2012), A physically based method for estimating supraglacial debris thickness from thermal band remote-sensing data, *J. Glaciol.*, *58*(210), 677–691, doi:10.3189/2012JoG11J194.
- Fujita, K., and A. Sakai (2014), Modelling runoff from a Himalayan debris-covered glacier, *Hydrol. Earth Syst. Sci.*, *18*(7), 2679–2694, doi:10.5194/hess-18-2679-2014.
- Fyffe, C. L., D. Tim, B. W. Brock, M. P. Kirkbride, G. Diolaiuti, C. Smiraglia, and F. Diotri (2014), A distributed energy-balance melt model of an alpine debris-covered glacier, *J. Glaciol.*, *60*(221), 587–602, doi:10.3189/2014JoG13J148.
- Guo, X., K. Yang, L. Zhao, W. Yang, S. Li, M. Zhu, T. Yao, and Y. Chen (2011), Critical evaluation of scalar roughness length parametrizations over a melting valley glacier, *Boundary Layer Meteorol.*, *139*(2), 307–332, doi:10.1007/s10546-010-9586-9.
- Immerzeel, W., P. Kraaijenbrink, J. Shea, A. Shrestha, F. Pellicciotti, M. Bierkens, and S. de Jong (2014), High-resolution monitoring of Himalayan glacier dynamics using unmanned aerial vehicles, *Remote Sens. Environ.*, *150*, 93–103, doi:10.1016/j.rse.2014.04.025.
- Inoue, J., and M. Yoshida (1980), Ablation and heat exchange over the Khumbu Glacier, *Seppyo J. Jpn. Soc. Snow Ice*, *41*, 26–33, doi:10.5331/seppyo.41.Special_26.
- Iqbal, M. (1983), *An Introduction to Solar Radiation*, 390 pp., Academic Press, New York.
- Irvine-Fynn, T. D., E. Sanz-Ablanedo, N. Rutter, M. W. Smith, and J. H. Chandler (2014), Measuring glacier surface roughness using plot-scale, close-range digital photogrammetry, *J. Glaciol.*, *60*(223), 957–969, doi:10.3189/2014JoG14J032.
- Iwata, S., O. Watanabe, and H. Fushimi (1980), Surface morphology in the ablation area of the Khumbu glacier, *Seppyo J. Jpn. Soc. Snow Ice*, *41*, 9–17.
- Janke, J. R., A. C. Bellisario, and F. A. Ferrando (2015), Classification of debris-covered glaciers and rock glaciers in the Andes of central Chile, *Geomorphology*, *241*, 98–121, doi:10.1016/j.geomorph.2015.03.034.
- Juszak, I., and F. Pellicciotti (2013), A comparison of parameterizations of incoming longwave radiation over melting glaciers: Model robustness and seasonal variability, *J. Geophys. Res. Atmos.*, *118*, 3066–3084, doi:10.1002/jgrd.50277.
- King, J. C., and P. S. Anderson (1994), Heat and water vapour fluxes and scalar roughness lengths over an Antarctic ice shelf, *Boundary Layer Meteorol.*, *69*(1–2), 101–121, doi:10.1007/BF00713297.
- Kraaijenbrink, P., S. W. Meijer, J. M. Shea, F. Pellicciotti, S. M. D. E. Jong, and W. W. Immerzeel (2016), Seasonal surface velocities of a Himalayan glacier derived by automated correlation of unmanned aerial vehicle imagery, *Ann. Glaciol.*, *57*(71), 103–113, doi:10.3189/2016AoG71A072.
- Lejeune, Y., J.-M. Bertrand, P. Wagnon, and S. Morin (2013), A physically based model of the year-round surface energy and mass balance of debris-covered glaciers, *J. Glaciol.*, *59*(214), 327–344, doi:10.3189/2013JoG12J149.
- Lettau, H. H. (1969), Note on aerodynamic roughness-parameter estimation on the basis of roughness-element description, *J. Appl. Meteorol.*, *8*, 828–832, doi:10.1175/1520-0450(1969)008<0828:NOARPE>2.0.CO;2.
- Liang, J., L. Zhang, Y. Wang, X. Cao, Q. Zhang, H. Wang, and B. Zhang (2014), Turbulence regimes and the validity of similarity theory in the stable boundary layer over complex terrain of the Loess Plateau, China, *J. Geophys. Res. Atmos.*, *119*, 6009–6021, doi:10.1002/2014JD021510.
- Martins, C. A., O. L. L. Moraes, O. C. Acevedo, and G. A. Degrazia (2009), Turbulence intensity parameters over a very complex terrain, *Boundary Layer Meteorol.*, *133*(1), 35–45.
- Miles, E., J. Steiner, F. Brun, P. Buri, F. Pellicciotti, I. Rico, and P. Hill (2017a), Micrometeorology and surface topography of debris-covered Lirung Glacier, Nepal, October–November 2014, Mendeley Data, v1, doi:10.17632/m2g3mg4364.1.
- Miles, E., I. C. Willis, N. S. Arnold, J. F. Steiner, and F. Pellicciotti (2017b), Spatial, seasonal, and interannual variability of supraglacial ponds in the Langtang Valley of Nepal, 1999 to 2013, *J. Glaciol.*, *237*, 88–105, doi:10.1017/jog.2016.120.
- Moore, R. D. (1983), On the use of bulk aerodynamic formulae over melting snow, *Nordic Hydrol.*, *14*(4), 193–206, doi:10.2166/nh.1983.016.
- Munro, D. S. (1989), Surface roughness and bulk heat transfer on a glacier: Comparison with eddy correlation, *J. Glaciol.*, *35*(121), 343–348.

- Nicholson, L., and D. I. Benn (2006), Calculating ice melt beneath a debris layer using meteorological data, *J. Glaciol.*, *52*(178), 463–470, doi:10.3189/172756506781828584.
- Nield, J. M., R. C. Chiverrell, S. E. Darby, J. Leyland, L. H. Vircavs, and B. Jacobs (2013a), Complex spatial feedbacks of tephra redistribution, ice melt and surface roughness modulate ablation on tephra covered glaciers, *Earth Surf. Processes Landforms*, *38*(1), 95–102, doi:10.1002/esp.3352.
- Nield, J. M., et al. (2013b), Estimating aerodynamic roughness over complex surface terrain, *J. Geophys. Res. Atmos.*, *118*, 12,948–12,961, doi:10.1002/2013JD020632.
- Østrem, G. (1959), Ice melting under a thin layer of moraine, and the existence of ice cores in moraine ridges, *Geogr. Ann.*, *41*(4), 228–230.
- Pellicciotti, F., C. Stephan, E. Miles, S. Herreid, W. W. Immerzeel, and T. Bolch (2015), Mass-balance changes of the debris-covered glaciers in the Langtang Himal, Nepal, from 1974 to 1999, *J. Glaciol.*, *61*(226), 373–386, doi:10.3189/2015JG13J237.
- Petersen, R. L. (1997), A wind tunnel evaluation of methods for estimating surface roughness length at industrial facilities, *Atmos. Environ.*, *31*(1), 45–57, doi:10.1016/S1352-2310(96)00154-9.
- Quincey, D. J., M. W. Smith, D. R. Rounce, A. Ross, O. King, and C. S. Watson (2017), Evaluating morphological estimates of the aerodynamic roughness of debris covered glacier ice, *Earth Surf. Processes Landforms*, doi:10.1002/esp.4198, in press.
- Ragetti, S., F. Pellicciotti, W. W. Immerzeel, E. S. Miles, L. Petersen, M. Heynen, J. M. Shea, D. Stumm, S. Joshi, and A. Shrestha (2015), Unraveling the hydrology of a Himalayan catchment through integration of high resolution in situ data and remote sensing with an advanced simulation model, *Adv. Water Resour.*, *78*, 94–111, doi:10.1016/j.advwatres.2015.01.013.
- Rees, W., and N. Arnold (2006), Scale-dependent roughness of a glacier surface: Implications for radar backscatter and aerodynamic roughness modelling, *J. Glaciol.*, *52*(177), 214–222, doi:10.3189/172756506781828665.
- Reid, T. D., and B. W. Brock (2010), An energy-balance model for debris-covered glaciers including heat conduction through the debris layer, *J. Glaciol.*, *56*(199), 903–916, doi:10.3189/002214310794457218.
- Reid, T. D., M. Carenzo, F. Pellicciotti, and B. W. Brock (2012), Including debris cover effects in a distributed model of glacier ablation, *J. Geophys. Res.*, *117*, D18105, doi:10.1029/2012JD017795.
- Rippin, D. M., A. Pomfret, and N. King (2015), High resolution mapping of supra-glacial drainage pathways reveals link between micro-channel drainage density, surface roughness and surface reflectance, *Earth Surf. Processes Landforms*, *40*, 1279–1290, doi:10.1002/esp.3719.
- Rounce, D. R., D. J. Quincey, and D. C. McKinney (2015), Debris-covered glacier energy balance model for Imja-Lhotse Shar glacier in the Everest region of Nepal, *Cryosphere*, *9*, 1–16, doi:10.5194/tc-9-1-2015.
- Sauter, T., and S. P. Galos (2016), Effects of local advection on the spatial sensible heat flux variation on a mountain glacier, *Cryosphere*, *10*, 2887–2905, doi:10.5194/tc-2016-139.
- Shao, Y., and Y. Yang (2008), A theory for drag partition over rough surfaces, *J. Geophys. Res.*, *113*, F02S05, doi:10.1029/2007JF000791.
- Shaw, T., B. Brock, C. Fyffe, F. Pellicciotti, N. Rutter, and F. Diotri (2015), Air temperature distribution and energy balance modelling of a debris-covered glacier, *J. Glaciol.*, *62*(23), 185–198, doi:10.1017/jog.2016.31.
- Sicart, J., M. Litt, W. D. Helgason, V. Tahar, and T. Chaperon (2014), A study of the atmospheric surface layer and roughness lengths on the high-altitude tropical Zongo glacier, Bolivia, *J. Geophys. Res. Atmos.*, *119*, 3793–3808, doi:10.1002/2014JD021494.
- Smeets, C. J. P. P., and M. R. van den Broeke (2008a), The parameterisation of scalar transfer over rough ice, *Boundary Layer Meteorol.*, *128*(3), 339–355, doi:10.1007/s10546-008-9292-z.
- Smeets, C. J. P. P., and M. R. van den Broeke (2008b), Temporal and spatial variations of the aerodynamic roughness length in the ablation zone of the Greenland ice sheet, *Boundary Layer Meteorol.*, *128*(3), 315–338, doi:10.1007/s10546-008-9291-0.
- Smeets, C. J. P. P., P. G. Duynkerke, and H. F. Vugts (1999), Observed wind profiles and turbulence fluxes over an ice surface with changing surface roughness, *Boundary Layer Meteorol.*, *92*, 101–123.
- Smith, M. W. (2014), Roughness in the Earth sciences, *Earth Sci. Rev.*, *136*, 202–225, doi:10.1016/j.earscirev.2014.05.016.
- Smith, M., J. Carrivick, and D. Quincey (2015a), Structure from motion photogrammetry in physical geography, *Prog. Phys. Geogr.*, *40*, 247–275, doi:10.1177/0309133315615805.
- Smith, M. W., D. J. Quincey, T. Dixon, R. G. Bingham, J. L. Carrivick, T. D. L. Irvine-Fynn, and D. M. Rippin (2015b), Aerodynamic roughness of glacial ice surfaces derived from high-resolution topographic data, *J. Geophys. Res. Earth Surf.*, *121*, 748–766, doi:10.1002/2015JF003759.
- Steiner, J., and F. Pellicciotti (2016), Variability of air temperature over a debris-covered glacier in the Nepalese Himalaya, *Ann. Glaciol.*, *57*(71), 295–307, doi:10.3189/2016AoG71A066.
- Steiner, J. F., F. Pellicciotti, P. Buri, E. S. Miles, W. W. Immerzeel, and T. D. Reid (2015), Modeling ice cliff backwasting on a debris covered glacier in the Nepalese Himalayas, *J. Glaciol.*, *61*(229), 889–907, doi:10.3189/2015JG14J194.
- Takeuchi, Y., R. B. Kayastha, and M. Nakawo (2000), Characteristics of ablation and heat balance in debris-free and debris-covered areas on Khumbu Glacier, Nepal Himalayas, in the pre-monsoon season, *IAHS Publ.*, *264*, 53–61.
- Thompson, S., D. I. Benn, J. Mertes, and A. Luckman (2016), Stagnation and mass loss on a Himalayan debris-covered glacier: Processes, patterns and rates, *J. Glaciol.*, *62*(233), 467–485, doi:10.1017/jog.2016.37.
- Wang, Y., J. Yao, H. Han, and S. Liu (2014), Analysis of aerodynamic roughness on Koxkar Glacier moraine surfaces, *Plateau Meteorol.*, *33*(3), 762–768, doi:10.7522/j.issn.1000-0534.2013.00140.
- Westoby, M. J., J. Brasington, N. F. Glasser, M. J. Hambrey, and J. M. Reynolds (2012), 'Structure-from-Motion' photogrammetry: A low-cost, effective tool for geoscience applications, *Geomorphology*, *179*, 300–314, doi:10.1016/j.geomorph.2012.08.021.
- Wiernga, J. (1993), Representative roughness parameters for homogeneous terrain, *Boundary Layer Meteorol.*, *63*(4), 323–363, doi:10.1007/BF00705357.
- Yang, K., T. Koike, H. Fujii, K. Tamagawa, and N. Hirose (2002), Improvement of surface flux parametrizations with a turbulence-related length, *Q. J. R. Meteorol. Soc.*, *128*(584), 2073–2087, doi:10.1256/003590002320603548.
- Zilitinkevich, S., T. Elperin, N. Kleerorin, I. Rogachevskii, I. Esau, T. Mauritsen, and M. Miles (2008), Turbulence energetics in stably stratified geophysical flows: Strong and weak mixing regimes, *Q. J. R. Meteorol. Soc.*, *134*, 793–799, doi:10.1002/qj.264.